Pharmaceutical Research, Vol. 22, No. 12, December 2005 (© 2005)
DOI: 10.1007/s11095-005-8176-x

Research Paper

Cubosome Dispersions as Delivery Systems for Percutaneous Administration of Indomethacin

Elisabetta Esposito,[1] Rita Cortesi,[1,6] Markus Drechsler,[2] Lydia Paccamiccio,[3] Paolo Mariani,[3] Catia Contado,[4] Elisa Stellin,[1] Enea Menegatti,[1] Francesco Bonina,[5] and Carmelo Puglia[5]

Received May 30, 2005; accepted August 23, 2005

Purpose. The present study concerns the production and characterization of monooleine (MO) dispersions as drug delivery systems for indomethacin, taken as model anti-inflammatory drug.
Methods. Dispersions were produced by emulsification and homogenization of MO and poloxamer in water. Morphology and dimensional distribution of the disperse phase have been characterized by cryo-transmission electron microscopy and photon correlation spectroscopy, respectively. X-ray diffraction has been performed to determine the structural organization of the disperse phase. Sedimentation field flow fractionation (SdFFF) has been performed to investigate drug distribution in the dispersion. An *in vitro* diffusion study was conducted by Franz cell associated to stratum corneum epidermis membrane on cubosome dispersions viscosized by carbomer. *In vivo* studies based on skin reflectance spectrophotometry and tape stripping were performed to better investigate the performance of cubosome as indomethacin delivery system.
Results. Microscopy studies showed the coexistence of vesicles and cubosomes. X-ray diffraction revealed the presence of a bicontinuous cubic phase of spatial symmetry *Im3m* (Q^{229}). SdFFF demonstrated that no free drug was present in the dispersion. Indomethacin incorporated in viscosized MO dispersions exhibited a lower flux with respect to the analogous formulation containing the free drug in the aqueous phase and to the control formulation based on carbomer gel. Reflectance spectroscopy demonstrated that indomethacin incorporated into MO dispersions can be released in a prolonged fashion. Tape-stripping experiments corroborated this finding.
Conclusions. MO dispersions can be proposed as nanoparticulate systems able to control the percutaneous absorption of indomethacin.

KEY WORDS: cryo-TEM; cubosomes; reflectance spectroscopy; tape stripping; X-ray.

INTRODUCTION

Cubic liquid crystals are transparent and isotropic phases that are physically stable in excess water (1–4) representing a unique system for the production of pharmaceutical dosage forms (5–7). One application of cubic phase liquid crystals is the controlled release of selected water- and oil-soluble molecules (8).

The emulsification of cubic lipid phases in water results in the production of cubosomes that can be defined as nanoparticulate disperse systems characterized by high biocompatibility and bioadhesivity (9,10). Because of their properties, these versatile delivery systems can be administrable by different routes (such as orally, parenterally, or percutaneously) (11,12).

Cubosomes have been usually produced by means of methods involving high-energy input and time-consuming procedures (13–15). We have recently published a study about the production of monoglyceride-based dispersions by a simple processing technique based on emulsification of a disperse phase constituted of monoglyceride/Poloxamer 407 in water. This procedure enabled to produce dispersions presenting 72% of cubosomes and vesicles in the nanometer size range plus 28% of larger irregular particles (16).

A recent cryo-transmission electron microscopy (cryo-TEM) study has been performed to investigate the structural organization of the stratum corneum (17). The study has provided that the global cryo-electron density pattern of the stratum corneum keratin intermediate filament network resembles "inverted" cryo-transmission electron micrographs of cubic lipid/water phases. At this regard, a "cubic-like rod-packing symmetry" could be attributed to the stratum corneum (17). The observation that biological interface itself possesses a cubic architecture suggests that dermal application of cubosomes could possibly result in a stratum corneum–cubosome interaction. In this view, the develop-

[1] Dipartimento di Scienze Farmaceutiche, Università di Ferrara, Via Fossato di Mortara, 19, 44100 Ferrara, Italy.
[2] Macromolecular Chemistry II, University of Bayreuth, Bayreuth, Germany.
[3] Dipartimento di Scienze Applicate ai Sistemi Complessi e INFM, Università Politecnica delle Marche, Ancona, Italy.
[4] Dipartimento di Chimica, Università di Ferrara, Ferrara, Italy.
[5] Dipartimento di Scienze Farmaceutiche, Università di Catania, Catania, Italy.
[6] To whom correspondence should be addressed. (e-mail: crt@unife.it)

ment of cubosome-based dermal products seems particularly interesting.

Although cubosome structure has been well characterized by cryo-electron microscopy, X-ray, and NMR investigations (12,18,19), and despite the amazing properties of cubosomes as innovative drug carriers, little work has been performed at present to demonstrate their potential as delivery systems able to control drug release [20–22].

The aim of this work was to study the performance of cubosomes as innovative cutaneous delivery systems for indomethacin, chosen as model drug.

Indomethacin (IND) is a member of the nonsteroidal anti-inflammatory drug family widely used in the treatment of dermatitis and rheumatic diseases (23). Although oral therapy with IND is very effective, its clinical use is limited by its potential side effects (24) and its short elimination half-life (25). Several studies have been aimed at the development of an efficient means of IND topical administration to increase local soft-tissue and joint concentration, while reducing its systemic distribution to avoid side effects (26,27).

The first part of the present study describes the production and characterization of IND-containing monooleine (MO) dispersions, whereas the second part deals in an *in vitro* and an *in vivo* investigation aimed to describe the release modalities of IND after the administration of the dispersion on the skin.

Cryo-transmission electron microscopy, X-ray diffraction, photon correlation spectroscopy (PCS), and field flow fractionation technique (28) have been employed to characterize the MO dispersions.

IND's percutaneous absorption has been studied *in vitro* from three different formulations using excised human skin membranes [stratum corneum epidermis (SCE)] mounted into Franz cells. IND delivery into the skin was studied determining its *in vivo* topical anti-inflammatory activity after cutaneous application of MO containing forms. The ultraviolet B (UVB)-induced erythema was chosen as inflammatory model on healthy human volunteers and was monitored by reflectance visible spectrophotometry. Moreover, tape-stripping experiments have been performed on skin after topical administration of cubosomes to quantify IND's presence in the stratum corneum.

MATERIALS AND METHODS

Materials

The glyceryl monooleate RYLO MG 19 (MO) was a gift from Danisco Cultor (Grindsted, Denmark).

Poloxamer 407 ($PEO_{98}POP_{67}PEO_{98}$) was obtained from BASF (Ludwigshafen, Germany). Carbopol 934P (CTFA: Carbomer) was from BFGoodrich (Cleveland, OH, USA). Indomethacin (IND) and all other materials were purchased from Fluka Chemicals (Buchs, Switzerland).

Production of Dispersions

Production of dispersions was based on the emulsification of MO (4.5% w/w) and Poloxamer 407 (0.5% w/w) in water (90%, w/w), as described by Esposito *et al.* (16). In the present study, after emulsification, the dispersion was subjected to homogenization at 15,000 rev min^{-1} (Ultra Turrax, Janke & Kunkel, Ika-Werk, Sardo, Italy) at 60°C for 1 min; afterwards, it was cooled and maintained at room temperature in glass vials.

In the case of IND-containing dispersions, 60 mg of the drug (3% w/w with respect to the monooleine, 0.15% w/w with respect to the dispersion) was added to the molten MO–poloxamer solution and solubilized before adding to the aqueous solution.

The dispersion was then filtered through mixed esters cellulose membrane (0.6-μm pore size) to separate big MO–poloxamer aggregates. Both dispersion and filter were weighed. Finally, the filter was left to desiccate in an oven at 70°C for 12 h to eliminate as much as possible the amount of water taken up by the particles; afterwards, it was weighted.

Dispersion characterization as well as *in vitro* and *in vivo* experiments were performed on the MO dispersions after filtration, without taking into account the fraction of larger particles whose dimensions have been measured by laser diffraction (Horiba, LA-920, Horiba Ltd., Tokyo, Japan).

For *in vitro* and *in vivo* experiments, a blank MO formulation and free drug were used to prepare controls. In particular, a weighted amount of IND has been added to 50 ml of a filtered MO dispersion and subjected to magnetic stirring (250 rev min^{-1}) for 1 h.

Characterization of Dispersions

Cryo-Transmission Electron Microscopy

Samples were prepared at ambient conditions. A 27-μl drop of solution was placed on a pure thin bar 600-mesh TEM grid (Science Services, Munich, Germany). The drop was blotted with filter paper until it was reduced to a thin film (10–200 nm) spanning the hexagonal holes of the TEM grid. The sample was then vitrified by rapidly immersing into liquid ethane near its freezing point. The vitrified specimen was transferred to a Zeiss EM922 transmission electron microscope for imaging using a cryoholder (CT3500, Gatan, Munich, Germany). The temperature of the sample was kept below −175°C throughout the examination. Specimens were examined with doses of about 1000–2000 e/nm^2 at 200 kV. Images were recorded digitally by a charge-coupled device camera (Ultrascan 1000, Gatan) using an image processing system (GMS 1.4 software, Gatan).

Photon Correlation Spectroscopy

Particle size analysis of the dispersions was performed using a Zetasizer 3000 PCS (Malvern Instr., Malvern, England) equipped with a 5-mW helium neon laser with a wavelength output of 633 nm. Samples of filtered dispersions were diluted 1:9 v/v with demineralized water. Measurements were made at 25°C at an angle of 90° with a run time of at least 180 s. Data were interpreted using the method of cumulants.

X-ray Diffraction Measurements

Diffraction measurements were carried out using a Philips PW 1830 X-ray generator equipped with a Guinier-

type focusing camera operating in vacuum with a bent quartz crystal monochromator which selects for the K_α line (λ = 0.154 nm). Diffraction patterns were recorded on a stack of three Kodak DEF-392 films or using an INEL Curved Position Sensitive 120 detector. Samples were held in a vacuum tight cylindrical cell provided with thin Mylar windows. Diffraction data were collected at 25°C, controlling the temperature with a Haake F3 Thermostat with an accuracy of 0.1°C.

Few structural information were derived from X-ray diffraction patterns: once the symmetry of the lipid phase was found, the unit cell dimension *a* was calculated according to the Bragg's law as follows:

$$a = \left(h^2 + k^2 + l^2\right)^{1/2} \Big/ s_{hkl}$$

where $s_{hkl} = 2\sin\vartheta/\lambda$ with 2ϑ the scattering angle and λ (0.154 nm) the wavelength (2,16).

Drug Content of Dispersions

With the aim to quantify drug content of dispersions after production, a sample of filtered dispersion was diluted in methanol (1:9 v/v) and analyzed for IND content by high-performance liquid chromatography (HPLC) with the below reported procedure. For sedimentation field flow fractionation (SdFFF) and stability studies, the amount of IND detected by HPLC after filtration was taken as reference of the total amount of drug.

Sedimentation Field Flow Fractionation Analysis

A SdFFF system (Model S101, FFFractionation, Inc., Salt Lake City, UT, USA), described elsewhere (29), was employed to determine the size distribution of the particles (PSD) by converting the fractograms, i.e., the graphical results, assuming the particle density is known. The mobile phase was a 0.001% w/v solution of Poloxamer 407 in Milli-Q water (Millipore S.p.A., Vimodrone, Milan, Italy), flowing at 1.5 ml/min. The samples were injected after an appropriate dilution of the original suspensions. Collected fractions have been analyzed by HPLC to quantify IND content.

HPLC Procedure

High-performance liquid chromatography analyses were performed using a Perkin-Elmer apparatus (Series 200, Wellsley, MA, USA). Chromatography was performed following a slight modification of the method reported by Liu *et al.* (30). Elution was conducted with a mobile phase constituted of water (pH 3 adjusted with phosphoric acid) and acetonitrile 30:70 v/v, with a flow rate of 1 ml/min. Detection was performed at 254 nm. The retention time for IND was 4.1 min.

Stability Studies

To assess the physical stability of MO dispersions, some organoleptic and morphological aspects were investigated as a function of time. PCS studies were repeated at different time intervals (from 0 to 3 months from production) to evaluate possible variations of particle dimensional distribution. In addition, samples of dispersions were diluted with methanol (1:9 v/v) and analyzed by HPLC to detect IND content by time.

Production of Viscous Vehicle

After production and filtration, MO dispersions were processed to hydrogel. In particular, three different viscous formulations were prepared. Previously, a viscous gel was obtained swelling a weighted amount of carbomer (1% w/w) in deonized water for 12 h and adding an equal amount of triethanolamine up to pH 7. The obtained gel was then alternatively diluted with an appropriate amount of MO dispersion encapsulating IND, blank MO dispersion plus free IND, or an IND water suspension. The final viscous forms have been named A, B, and C, respectively. Namely, the ratio between the liquid formulation and the gel was 2:1 w/w, and the final concentration of carbomer was 0.3% w/w. The IND concentration in liquid formulations before the addition of carbomer gel was 0.1%, whereas the final IND concentration in the viscous forms was 0.07% w/w.

***In Vitro* Studies**

For *in vitro* diffusion studies, samples of adult human skin (mean age 36 ± 8 years) from breast reduction operations were employed. The epidermal membranes were dried in a desiccator at approximately 25% relative humidity (RH) and then stored in aluminum foil at 4 ± 1°C until use. Preliminary experiments were carried out to assess SCE samples for barrier integrity by measuring the *in vitro* permeability of [^{3}H] water through the membranes using the Franz cells described below. The value of the permeability coefficient (P_m) for tritiated water was found to be $1.6 \pm 0.2 \times 10^{-3}$ cm/h, which agreed well with those for tritiated water reported by others using human SCE samples (31).

Samples of dried SCE were rehydrated by immersion in distilled water at room temperature for 1 h before being mounted in Franz-type diffusion cells supplied by LGA (Berkeley, CA, USA). The exposed skin surface area was 0.75 cm^2, and the receiver compartment volume was of 4.5 ml.

The receptor compartment contained a water–ethanol solution (50:50 v/v) to allow the establishment of the "sink condition" and to sustain permeant solubilization (32). This solution was stirred with the help of a magnetic bar at 500 rpm and thermostated at 35 ± 1°C during all the experiments (33).

After placing approximately 100 mg of each gel formulation (A, B, C) on the skin surface, the donor compartment was sealed to avoid evaporation. Each experiment was run in duplicate for 36 h using three different donors (n = 3). At intervals (t = 0, 2, 4, 6, 8, 12, 18, 24, and 36 h), samples (200 μl) of receiving solution were withdrawn and replaced with fresh solution. The samples were analyzed for IND content by HPLC as described above. IND fluxes through the skin were calculated by plotting the cumulative amount of drug penetrating the skin against time and determining the slope of the linear portion of the curve and the χ-intercept values (lag time) by linear regression analysis. Drug fluxes

($\mu g/cm^2/h$), at steady state, were calculated by dividing the slope of the linear portion of the curve by the area of the skin surface through which diffusion took place.

In Vivo Studies

In vivo experiments were performed on two groups of ten volunteers: group A enrolled for the first *in vivo* experimentation (evaluation of anti-inflammatory activity) and group B enrolled for the second one (tape stripping). The volunteers were of both sexes in the age range 25–35 years and recruited after medical screening including filling in a health questionnaire followed by physical examination of the application sites. After they were fully informed of the nature of the study and of the procedures involved, they gave their written consent. The participants did not suffer from any ailment and were not on any medication at the time of the study. They were rested for 15 min prior to the experiments, and room conditions were set at 22 ± 2°C and 40–50% RH.

In Vivo Anti-inflammatory Activity

Ultraviolet-B-induced skin erythema was monitored by using a reflectance visible spectrophotometer X-Rite model 968 (X-Rite Inc. Grandville, MI, USA), calibrated and controlled as previously reported (34,35). The reflectance spectra were obtained over the wavelength range 400–700 nm using illuminant C and 2° standard observer. From the spectral data obtained, the erythema index (E.I.) was calculated using Eq. (1) (36):

$$E.I. = 100\left[\log\frac{1}{R_{560}} + 1.5\left(\log\frac{1}{R_{540}} + \log\frac{1}{R_{580}}\right) - 2\left(\log\frac{1}{R_{510}} + \log\frac{1}{R_{610}}\right)\right] \quad (1)$$

Skin erythema was induced by UVB irradiation using a UVM-57 ultraviolet lamp (UVP, San Gabriel, CA, USA) whose specific parameters are reported elsewhere (34). The minimal erythemal dose (MED) was preliminarily determined, and an irradiation dose corresponding to twice the value of MED was used throughout the study.

For each subject, ten sites on the ventral surface of each forearm were defined using a circular template (1 cm^2) and demarcated with permanent ink: one of the ten sites of each forearm was used as control, three sites were treated with 100 mg of formulation A, other three sites with 100 mg of formulation B, and, finally, the remaining three sites were treated with 100 mg of formulation C. The preparations were spread uniformly on the site by means of a solid glass rod. The sites were then occluded for 6 h using Hill Top Chambers (Hill Top Research, Cincinnati, OH, USA). After the occlusion period, the chambers were removed, and the skin surfaces were washed to remove the gel and allowed to dry for 15 min. Each pretreated site was exposed to UVB irradiation 1 h (t = 1) and 3 and 6 h (t = 3 and 6, respectively) after gel removal, and the induced erythema was monitored for 52 h. E.I. baseline values were taken at each designated site before application of gel formulation, and they were subtracted from the E.I. values obtained after UVB irradiation at each time point to obtain ΔE.I. values. For each site, the area under the response (ΔE.I)–time curve (AUC) was computed using the trapezoidal rule.

To better outline the results obtained, from AUC values, the percentage of inhibition of the erythema (P.I.E.) induced by UVB radiations was calculated using Eq. (2):

$$Inhibition\,(\%) = \frac{AUC_{(C)} - AUC_{(T)}}{AUC_{(C)}} \times 100 \quad (2)$$

where $AUC_{(C)}$ is the area under the response–time curve of the vehicle-treated site (control) and $AUC_{(T)}$ is the area under the response–time curve of the drug-treated site.

Tape Stripping

The first steps of the experimental protocol previously described were also employed in this second *in vivo* study; in fact, for each subject of group B, ten sites (2 cm^2) were defined on the ventral surface of each forearm, and 200 mg of each hydrogel formulations (A–C) was applied on these cutaneous sites (three sites of application for each formulation in duplicate). The preparations were spread uniformly on the site by means of a solid glass rod and were then occluded for 6 h. After the occlusion period, the residual formulations were removed by gently wiping with cotton balls (different for each pretreated site). Twenty individual 2-cm^2 squares of adhesive tape (Scotch Book Tape 845, 3M) were utilized to sequentially tape-strip the stratum corneum on the application sites. To obtain a realistic comparison between the results of this experimentation and the ones obtained in the previous *in vivo* study, the removal of stratum corneum in each pretreated site was effected at 1 h (t = 1) and 3 and 6 h (t = 3 and 6, respectively) after gel removal.

Each adhesive square, before and after skin tape stripping, was weighed on a Sartorius balance (model ME415S, sensitivity 1 μg) to quantify the weight of stratum corneum removed. Then each tape strip was extracted over 16 h with acetonitrile and submitted to HPLC to determine the IND content. The recovery of IND was validated by spiking tape-stripped samples of untreated stratum corneum with 100 μl of a 10-mg/ml solution of IND in acetonitrile (approximately 1 mg/tape of IND). The extraction efficiency was 91.3 ± 0.6% of IND (n = 3).

Statistical Analysis

Statistical analysis of *in vitro* data was performed using Student's t test. Statistical differences of *in vivo* data are determined using repeated-measures analysis of variance (ANOVA) followed by the Bonferroni–Dunn *post hoc* pairwise comparison procedure. A probability p of less than 0.05 is considered significant in this study.

RESULTS

Production of Monoglyceride-Based Dispersions

To produce MO dispersions reducing the presence of larger irregular particles, in the present investigation, the

emulsification method described by Esposito *et al.* (16) was followed by hot homogenization (37).

The weight of dispersion, calculated while taking into account the loss of dispersing phase because of water evaporation, was found to be 90 ± 0.01% with respect to water–MO–poloxamer weight before production. Thus, the extent of water loss (calculated by difference) was 10 ± 0.01%.

The weight of the larger particles after filtration and desiccation was 10 ± 0.5% with respect to the MO–poloxamer weight before production.

It was found that the IND concentration in the filtered dispersion was 0.1 ± 0.02% w/w with respect to the weight of the filtered dispersion (88% w/w, with respect to the weight of the drug employed). All data were the mean of eight determinations on different batches of the same type of dispersion.

Characterization of Dispersions

To investigate the internal structure of the dispersed particles in monooleine-based dispersions and to detect possible variation because of the presence of IND, cryo-TEM analyses have been conducted. Figure 1 shows images

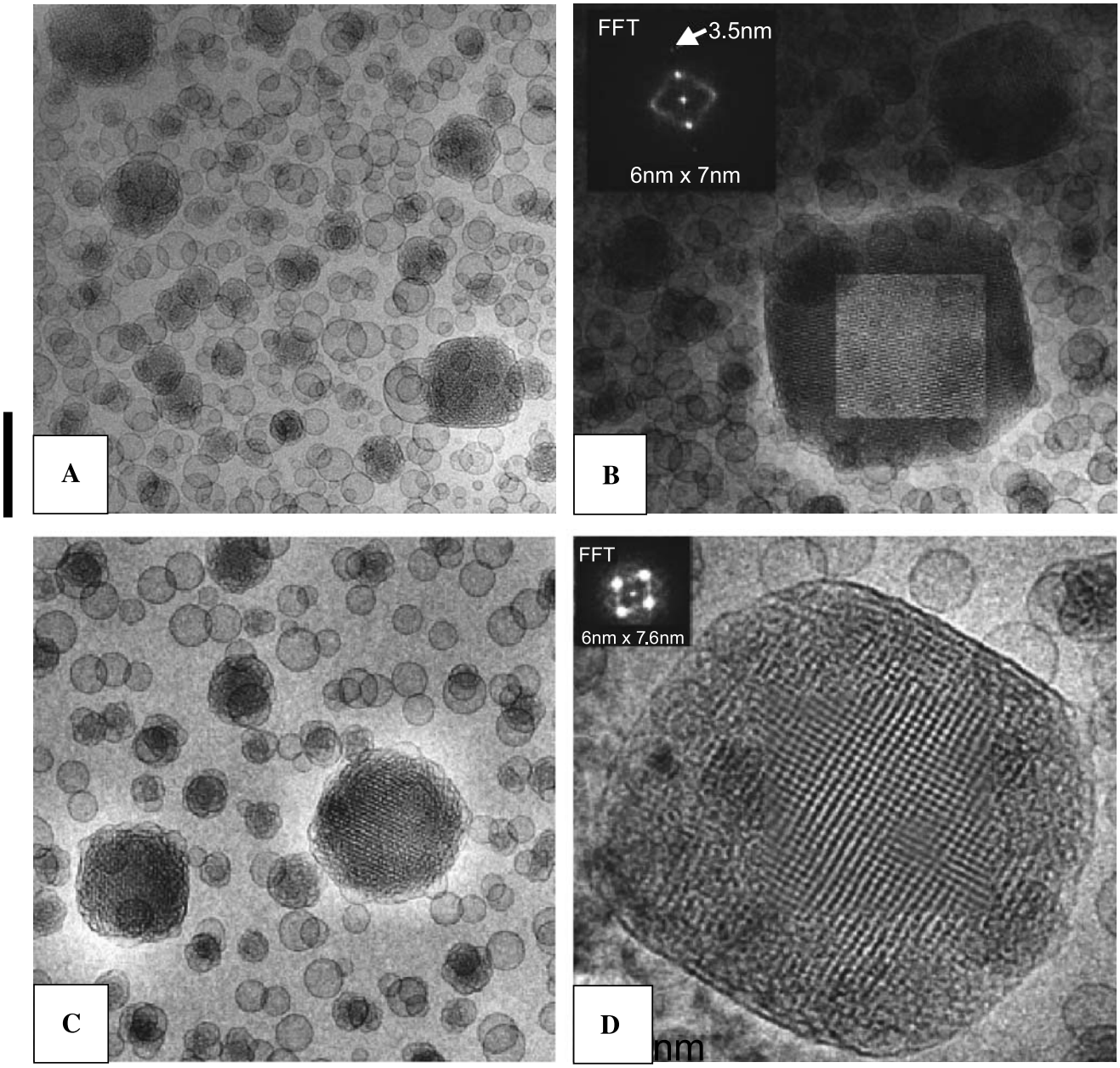

Fig. 1. Panels A, B: Cryo-transmission electron microscopy (cryo-TEM) micrographs of placebo monooleine dispersion. Panels C, D: Cryo-TEM micrographs of indomethacin (IND) monooleine dispersion. The inset of panel B shows the diameter of the aqueous channel (indicated by the white arrow) and the spacing of the unit cell. The bar equals 200 nm in panel A, 150 nm in panels B and C, and 60 nm in panel D. The disperse phase constituted of monooleine/Poloxamer 407 90:10 w/w; the disperse phase/dispersing phase ratio was 5:95; the dispersion was produced by mechanical stirring followed by hot homogenization.

taken from monooleine dispersions in the absence (panels A and B) and in the presence of IND (panels C and D). Vesicles and well-shaped cubosomes, exhibiting the typical ordered cubic texture, can be observed both in the placebo and in the drug containing dispersions. The inset of panel B shows a spacing of a repeat unit of 6 × 7 nm, indicating a tilt of the cubosome. The 3.5-nm spot indicates the diameter of the intercalating cubosomal aqueous channel. The presence of IND does not seem to affect the ultrastructure of the disperse phase. Panels A and C show the presence of vesicular structures attached on the surface of cubosomes, as found in cryo-TEM and X-ray studies reported by other authors, suggesting that through time, a transformation may take place from conglomerates of partially fused vesicles to well-ordered particles (15,19).

More than 100 pictures were taken from cryo-Tem observation, both for blank or IND-containing monooleine dispersions (data not shown); dimensions have been measured by a scale bar, finding that two different populations were present: one constituted of large cubosomes (dimensions over 200 nm) and another of smaller cubosomes and vesicles with dimensions about 100 nm and below. The dimensions of the larger particles separated by filtration ranged between 25 and 30 μm, as measured by laser diffraction.

Table I summarizes the results of PCS studies conducted to determine the dimensional distribution of monooleine dispersions. Dispersions were characterized by a monomodal dimensional distribution and an intensity mean diameter of 198.2 nm, expressed as *Z* average (Table I). IND slightly increased the mean diameter of nanostructures, passing to 206.7 nm in the presence of the drug. The analysis by number revealed that the most representative amount of nanoparticles/vesicles (percentage of peak area, 99.7 and 99.8%) displayed a mean diameter of 78 nm in the case of empty dispersions and 96 nm in the case of IND encapsulating ones.

X-ray Diffraction Analyses

X-ray diffraction experiments have been performed on MO dispersions with the aim to determine the structural organization. A series of diffraction profiles, obtained respectively in the absence and in the presence of IND, are reported in Fig. 2.

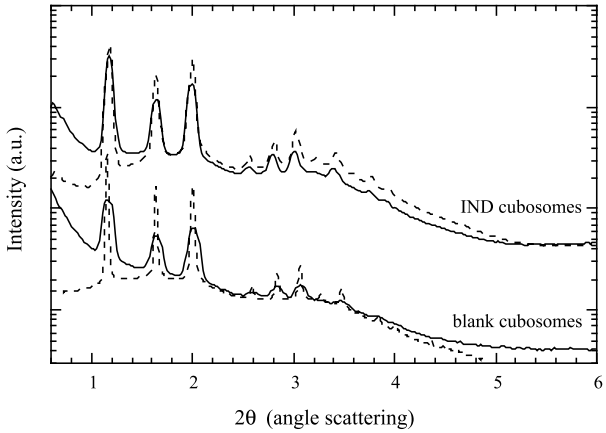

Fig. 2. Small angle X-ray diffraction profiles of a monooleine–poloxamer dispersion prepared in the absence and in the presence of IND. The dotted line represents the X-ray diffraction patterns measured after 3 months from the sample preparation.

Several Bragg peaks are observed in both samples. The spacing ratio of reflections (√2:√4:√6:√8:√10...) are consistent with the formation of a bicontinuous cubic phase of *Im3m* symmetry (Q^{229}). This phase is characterized by two 3-D networks formed by rods orthogonally connected 6 × 6. A diffuse low-angle scattering, which can be related to the presence of large micelles and/or vesicles, is also observed. X-ray diffraction qualitative results are in full agreement with cryo-TEM observations (Fig. 1), which reveal the coexistence of vesicles and particles characterized by a cubic organization. Noticeable is the fact that in the absence and in the presence of IND, the samples reveal a similar cubic unit cell dimension, being 10.8 nm for blank cubosomes and 10.6 nm for IND cubosomes. Even if the small reduction of the unit cell could be related to the presence of the drug, the analysis of the peak intensity profile shows that the IND does not remarkably alter the cubosome structure. From the unit cell,

Table I. Mean Diameter and Effect of Aging of Monooleine (MO)-Based Dispersions in the Absence and in the Presence of Indomethacin (IND)

Days	Monooleine dispersion	Mean diameter *Z* average[a] (nm) ± SD	P.I.[b] ± SD	Analysis by number		
				Peak area (%)	Mean diameter (nm)	Width
0	Blank dispersion	198.2 ± 2.1	0.18 ± 0.03	99.7 ± 0.1	78.0 ± 0.2	6.9 ± 0.3
	IND dispersion	206.7 ± 0.5	0.13 ± 0.02	99.8 ± 0.1	95.6 ± 0.3	20.5 ± 0.2
30	Blank dispersion	201.8 ± 1.8	0.19 ± 0.06	95.5 ± 0.2	88.1 ± 0.3	28.0 ± 0.1
	IND dispersion	205.3 ± 0.8	0.08 ± 0.05	95.7 ± 0.2	101.3 ± 0.4	30.5 ± 0.1
60	Blank dispersion	202.2 ± 0.9	0.15 ± 0.02	90.7 ± 0.1	102.4 ± 0.2	27.5 ± 0.1
	IND dispersion	210.1 ± 1.7	0.25 ± 0.03	90.9 ± 0.1	104.3 ± 0.1	24.6 ± 0.4
90	Blank dispersion	204.8 ± 0.7	0.19 ± 0.02	87.9 ± 0.1	103.2 ± 0.2	30.1 ± 0.2
	IND dispersion	211.5 ± 1.4	0.22 ± 0.04	86.9 ± 0.2	102.5 ± 0.1	31.2 ± 0.1

SD: standard deviation.
Photon correlation spectroscopy (PCS) data were the mean of five determinations of different batches of the same type of dispersion. Dispersions were produced by a disperse phase constituted of monooleine/Poloxamer 407 90:10 w/w in water with a 5:95 disperse phase/dispersing phase ratio.
[a] Determined by PCS.
[b] Polydispersity index.

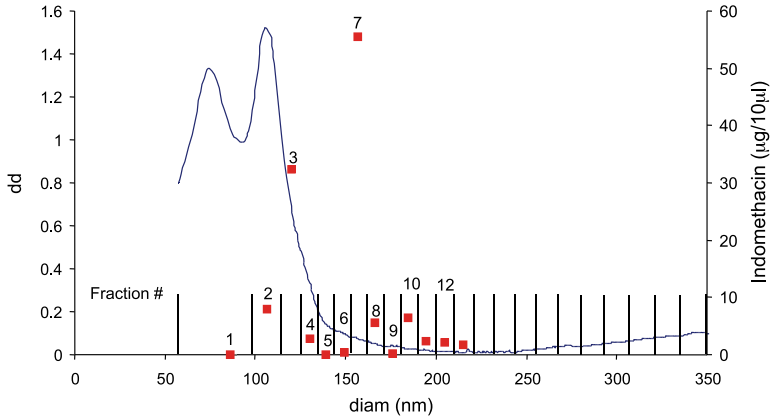

Fig. 3. PSD elaborated from the SdFFF fractogram. Particles were assumed to have a density of 1.04 g/ml (diam = diameter of nanoparticles; dd = dimensional distribution; the red dots indicate indomethacin content, as determined by high-performance liquid chromatography, and the vertical lines indicate the collected fractions).

it can be deduced that the 2-D periodically ordered (7 × 6 nm) domains observed by cryomicroscopy are normal to the [110] crystallographic axis of the cubic unit cell. The small differences observed between the repeat unit measured by cryomicroscopy (6–7 nm) and the spacing obtained from X-ray diffraction (7.6 nm) could be attributed to the shrinking of the cubosome during cryo procedures.

From X-ray diffraction data, assuming distinct water and lipid regions within the cell, the radius of the aqueous channels in the *Im3m* cubic phase has been also deduced from analytical equations reported elsewhere (2,3). By assuming a lipid hydration around 40%, as for pure MO in excess of water (2), radii of 1.81 and 1.77 nm have been estimated for blank and IND-containing samples, respectively. These values are in very good agreement with the dimension for the aqueous channels obtained by cryo-TEM images.

It should be finally observed that X-ray diffraction experiments have been repeated on the same samples after 3 months: the obtained profiles indicate a strong stability of the cubic structure (which maintains the same unit cell and intensity profile), which suggests that the amount of vesicles reduces as a function of time, as indicated by the reduced low-angle diffuse scattering.

Sedimentation Field Flow Fractionation Analyses

After filtration, both gel permeation chromatography and centrifugation were performed in an attempt to separate the free drug from the dispersions; nevertheless, no method was found suitable for IND separation. SdFFF has been employed as an alternative system. SdFFF should give information about the size distribution of the disperse phase and about the IND distribution in the dispersions. The fractogram obtained by SdFFF can be converted into a PSD plot, i.e., the amount of material per unit change of diameter, according to well-proven equations, by transforming the retention time in diameter of a sphere and the UV signal into a mass frequency function (38–40). In addition, the collected fractions can be analyzed by HPLC to quantify the amount of drug contained in the different populations of the disperse phase.

Figure 3 shows the PSD plot of a diluted amount of IND-containing monooleine dispersion. The conversion has been performed by assuming a density of 1.04 mg/ml. Also reported in the same graph is the concentration of IND determined by HPLC.

The fraction collected in correspondence of the void peak does not contain the drug, which is instead found in correspondence of the retained peak in the fractogram. Fractions 2–4 contain 39% of the total drug. The sizes of the components existing in this zone have a maximum of about 107 nm. It is known from cryo-TEM and PCS analyses that monooleine dispersions are mainly characterized by vesicles and small cubosomes with mean diameter around 100 nm, whereas a few cubosomes with larger dimensions are also present. Fractions 7 and 8 contain a high percentage of IND (roughly 50%), even if from the fractograms no particular population of particles is found. The remaining 11% of IND has been found in fractions 10–13, again not corresponding to any evidenced population of particles.

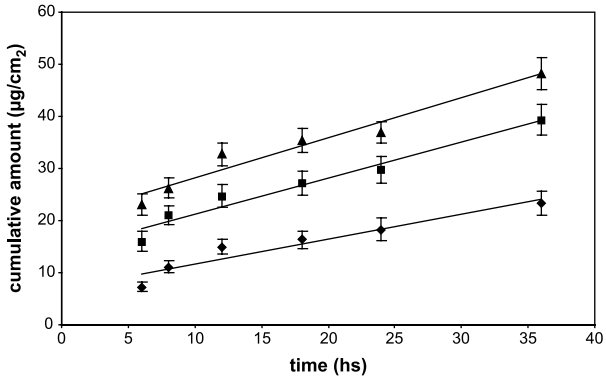

Fig. 4. *In vitro* diffusion of IND from carbomer gel (triangles), viscosized monooleine dispersion plus free IND (squares), and viscosized monooleine dispersion (rhombs), as determined by Franz cell system assembled with human skin.

Table II. AUC_{0-52} Values Obtained Pretreating Skin Sites with Different Topical Formulations (A–C) Containing Indomethacin (0.07%) and Applying Ultraviolet B Radiations after 1 h ($t = 1$), 3 h ($t = 3$), or 6 h ($t = 6$) from Their Removal

	AUC_{0-52}									
	$t = 1$			$t = 3$			$t = 6$			
Subjects	Form A	Form B	Form C	Form A	Form B	Form C	Form A	Form B	Form C	Control
A	1141.7	896.2	604.3	619.3	887.2	704.8	620.4	818.2	921.6	1321.6
B	828.6	716.2	443.2	395.6	850.1	724.3	428.6	768.9	860.1	955.6
C	904.1	629.7	506.3	835.1	798.4	994.3	861.3	1003.9	1184.6	1298.6
D	824.9	700.5	698.3	629.9	893.6	890.6	736.4	994.8	991.1	1221.4
E	719.4	628.3	527.1	593.4	804.6	788.6	636.8	921.6	965.4	1025.6
F	273.2	376.2	218.7	255.4	204.1	330.4	398.4	383.6	405.3	453.9
G	671.9	528.4	623.5	600.1	823.4	821.7	618.2	883.4	1038.6	1214.2
H	798.6	625.3	511.2	598.4	799.5	883.4	700.6	988.6	986.4	1210.1
I	952.4	786.7	688.9	695.2	896.4	987.2	698.6	1122.1	994.8	1158.7
L	1234.6	1128.1	900.4	954.3	1146.5	1028.4	860.2	1216.2	1319.5	1436.4
Mean	834.9	701.6	572.2	617.7	810.4	815.4	654.0	910.1	966.7	1129.6

A: MO dispersion encapsulating IND viscosized with carbomer; B: blank MO dispersion plus free IND viscosized with carbomer; C: IND carbomer gel.

Stability Studies

The organoleptic and morphological aspects of dispersions do not change through time, being free from phase separation phenomena for almost 1 year from production.

As reported in Table I, monooleine dispersions, in the presence and in the absence of IND, maintain their dimensions after 1 month; afterwards, mean diameters slightly increased in the succeeding 2 months. It is interesting to stress that the percentage of the number of nanostructures with the lowest diameter decreases from 99% at time 0 to 95, 90, and 87% after 1, 2, and 3 months, respectively, from production. The amount of IND in filtered monooleine dispersions determined by HPLC is almost quantitative also after 3 months from production, being 96.4 ± 0.1% with respect to the amount of drug found after production and filtration. This datum is the mean of five independent determinations. Moreover, the unvaried shape and retention time of IND peak and the absence of secondary peaks in the HPLC chromatograms (data not shown) demonstrate that IND was not degraded also after 3 months of storage at room temperature.

In Vitro Indomethacin Diffusion Study

In Fig. 4, the plots of the cumulative amounts of IND permeated through human SCE membranes as a function of time are shown. The flux values of IND from hydrogels A–C were calculated from the linear segments at the steady state. IND flux from A (0.63 ± 0.11 μg/cm^2) was the lowest, followed by the flux of the drug incorporated in B (0.92 ± 0.15 μg/cm^2) and by the flux of the drug incorporated in C (1.02 ± 0.18 μg/cm^2). Statistical analysis revealed no significant differences between the steady-state flux value obtained with the formulation containing MO dispersion and free IND (hydrogel B) and the value registered with hydrogel C ($p > 0.05$). Moreover, both B and C formulations showed flux values significantly higher than A formulation ($p < 0.05$).

Because the pH and the viscosity of vehicles have been shown to be important variables that could influence diffusivity of drugs in semisolid vehicles (41), these values were measured for A, B, and C forms. Both pH and viscosity were very close for the different forms, being 6.50 (A), 6.45 (B), and 6.53 (C) for the pH values and, at 60-s^{-1} shear

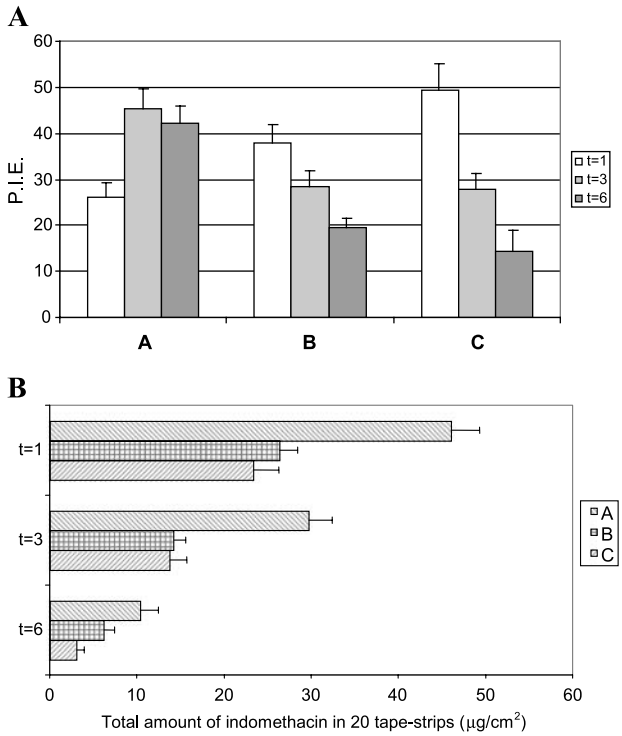

Fig. 5. *In vivo* comparative study of IND anti-inflammatory effect (panel A) and IND amount in the stratum corneum (panel B) after topical application and removal of different forms. P.I.E: percentage of erythema index; $t = 1$, 3, and 6: hours from the removal of formulations. A: IND containing viscosized monooleine dispersion, B: viscosized monooleine dispersion plus free IND, C: IND containing carbomer gel.

rate, 1650 (A), 1600 (B), and 1630 (C) cps for the viscosity values.

In Vivo Evaluation of Indomethacin Percutaneous Absorption

Indomethacin Anti-Inflammatory Effect

The IND percutaneous absorption from A–C forms was evaluated *in vivo* by monitoring in a noninvasive manner (42) the effect on an UVB-induced erythema, following a procedure reported in previous studies (34,43). An inverse relationship was found between the AUC and the inhibition of UVB-induced erythema (see Table II). UVB erythema induction was carried out at different times (1, 3, and 6 h; t = 1, 3, and 6, respectively) after A–C topical formulation removal. As reported in Table II, at t = 1, formulation C was more effective than forms A and B in inhibiting the induced erythema ($p < 0.05$). In particular, form A showed a significant inhibitory activity at t = 3 and 6 ($p > 0.05$).

P.I.E. values are reported in Fig. 5. Formulations B and C showed a similar anti-inflammatory profile; in particular, formulation C inhibition was maximal at t = 1, whereas it noticeably decreased at t = 3 and it was about 10% after 6 h (t = 6) from gel removal. Formulation B, containing a MO dispersion and free IND, provided, after 3 (t = 3) and 6 h (t = 6), AUC values not significantly different ($p > 0.05$) with respect to formulation C. As reported in Fig. 5, panel A, the anti-inflammatory profile of formulation A seemed remarkably different compared to the other formulations: in fact, at t = 1, P.I.E. was about 25%, and consequently, it was lower than the P.I.E. value registered for formulations B and C (38 and 50%, respectively), whereas it increased to about 45% at t = 3 and it was about 42% at t = 6.

Tape Stripping

Approximately the same amount of stratum corneum was removed with each tape strips from the treated sites of the three viscous formulations (A–C). The cumulative amount of stratum corneum removed from the tape stripping increased more rapidly in the initial three to ten strips and gradually reached a linear profile for the latter strippings (data not shown). The amount of IND recovered in the stratum corneum after 1 h (Fig. 5, panel B) from the removal of form A was noticeably higher than the amount of drug recovered after 1 h from the removal of the other two formulations ($p < 0.05$). Similar trends were observed also after 3 and 6 h from gel A removal, and the amounts of IND recovered from the strips showed appreciable variations ($p < 0.05$). On the contrary, the amount of IND recovered after 1, 3, and 6 h from the removal of gels B and C seemed not significantly different ($p > 0.05$).

DISCUSSION

A crucial point related to the characterization and to the employment of colloidal nanoparticulate systems, such as liposomes, solid lipid nanoparticles, and cubosomes, is the determination of the distribution of the drug within the dispersion. As a function of its solubility, the drug tends to associate partially to the matrix of the particulate systems, i.e., the disperse phase, and partially to be free in the aqueous dispersing phase. The performance of a drug delivery device should be tested taking into consideration only the encapsulated drug, after separation of the free one. The determination of the amount of free drug and its separation from the carrying system are often difficult procedures because of the complexity and heterogeneity of the nanodisperse systems. Ultrafiltration, dialysis, and gel permeation chromatography are some of the most employed methods.

In this study, to detect the possible amount of free IND in MO dispersions, firstly, gel permeation chromatography was unsuccessfully used. This failure could be due to a possible chemical–physical interaction between monooleine and the resin packaging of the column. This interaction should lead to a reduction of the elution rate until the complete obstruction of the column.

As a second attempt, SdFFF was employed. One major advantage of the SdFFF technique is that the analysis is a nondestructive sorting of the sample; moreover, the fractogram can be converted into a PSD plot (37–39).

From SdFFF analyses, it has been shown that IND is not free in the dispersion but is partially associated to a smaller diameter population (vesicles and little cubosomes) and partially to fractions corresponding to undetectable populations (Fig. 3). A plausible interpretation of these evidences is that the material eluted in the undetectable region has a heavier mass, which probably corresponds to a bigger size of the nanostructures or to a different arrangement of the chemical components that modify the density of the nanostructures. What is relevant is that these components are undetectable by turbidimetric methods (UV signal of the fractogram) because of their lower percentage with respect to the first population, but they contain a higher amount of drug. These findings are in agreement with X-ray diffraction analyses and cryo-TEM observations.

Because MO dispersions are dynamic changeable heterogeneous systems, it is to be noted that IND distribution between cubosomes and vesicles can change by time. X-ray and size data on aged dispersions corroborated the hypothesis that by time, a transformation takes place in the dispersions, where vesicles aggregate together, forming larger structures.

The results reported in Fig. 4 indicate that cubosome can control the diffusion of the incorporated drug. The higher flux of IND from B formulation with respect to the flux from A could account for the different distribution of the drug in the dispersion; free IND can diffuse more rapidly with respect to the drug incorporated in cubosomes and vesicles.

Moreover, the presence of blank cubosomes and vesicles slightly slows the IND diffusion with respect to control gel C, taking into account potential interactions between free IND and the lipid matrix of the nanostructures. Furthermore, this result outlined that the main factor controlling drug diffusion is the cubosome and vesicle presence, rather than the viscosity of the gel.

In vivo results reported in Fig. 5A demonstrate that drug incorporated in formulation A drastically influenced the lasting of anti-inflammatory activity and consequently IND prolonged release, whereas the anti-inflammatory effect exerted by formulations B and C is time limited.

Tape-stripping technique was useful for quantifying drug depletion in the viable epidermis and the amount of IND responsible for the anti-inflammatory effect. From the analysis of the data, the amount of IND recovered in the stratum corneum after 1 h from the removal of A hydrogel was high, but after 3 and 6 h, this amount strongly decreased (Fig. 5B). Because some authors have found a similarity between the cubic phase structure and the structure of the stratum corneum (17), it is reasonable to suppose the formation of a mix of cubosomal MO with stratum corneum lipids. This kind of interaction might lead to the formation of a cubosome depot in this layer from which IND can be released in a controlled fashion. Therefore, the variations of IND amounts revealed at different time points have to be ascribed to a drug slow release from this reservoir. The same amounts were probably responsible for the formulation A anti-inflammatory profile recorded.

CONCLUSIONS

A simple process, based on dispersion and homogenization of monooleine and poloxamer in water, leads to the formation of a complex heterogeneous system, suitable for the delivery of lipophilic drugs through the skin. The data here reported indicate a prolonged anti-inflammatory activity exerted by IND. The stratum-corneum-like structure attributed to cubosome by other authors (17) suggests the hypothesis of a cubosome depot effect on the epidermis. Nevertheless, further specialized studies are required to confirm this fascinating hypothesis and to better investigate the role of vesicles and cubosomes in controlling the release of the drug.

ACKNOWLEDGMENTS

This work was supported by the Ministry of Education, University and Research of Italy (MIUR), FIRB project.

REFERENCES

1. S. T. Hyde, S. Andersson, B. Ericsson, and K. Larsson. A cubic structure consisting of a lipid bilayer forming an infinite periodic minimal surface of the gyroid type in the glycerol monooleate water system. *Z. Kristallogr.* **168**:213–219 (1984).
2. P. Mariani, V. Luzzati, and H. Delacroix. Cubic phases of lipid-containing systems. Structure analysis and biological implications. *J. Mol. Biol.* **204**:165–189 (1988).
3. V. Luzzati, R. Vargas, P. Mariani, A. Gulik, and H. Delacroix. Cubic phases of lipid-containing systems. Elements of a theory and biological connotations. *J. Mol. Biol.* **229**:540–551 (1993).
4. H. Chung and M. Caffrey. The neutral area surface of the cubic mesophases: location and properties. *Biophys. J.* **66**:377–381 (1994).
5. P. D'Antona, W. O. Parker Jr., M. C. Zanirato, E. Esposito, and C. Nastruzzi. Rheologic and NMR characterization of monoglyceride-based formulation. *J. Biomed. Mater. Pharm.* **52**:40–52 (2000).
6. S. Engstroem, T. P. Norden, and H. Nyquist. Cubic phases for studies of drug partition into lipid bilayers. *Eur. J. Pharm.* **8**:243–254 (1999).
7. S. Engstroem, L. Lindahl, R. Wallin, and J. Engblom. A study of polar lipid drug carrier systems undergoing a thermoreversible lamellar-to-cubic phase transition. *Int. J. Pharm.* **86**:137–145 (1992).
8. J. C. Shah, Y. Sadhale, and D. M. Chilukuri. Cubic phase gels as drug delivery systems. *Adv. Drug Deliv. Rev.* **47**:229–250 (2001).
9. K. Larsson. Aqueous dispersion of cubic lipid–water phases. *Curr. Opin. Colloid Interface Sci.* **5**:64–69 (2000).
10. T. Landh and K. Larsson. Particles, method of preparing said particles and uses thereof. US patent no. 5531925 (1996).
11. J. Gustafsson, H. Ljusberg-Wharen, M. Almgrem, and K. Larsson. Submicronparticles of reversed lipid phases in water stabilized by a nonionic amphiphilic polymer. *Langmuir* **13**:6964–6971 (1997).
12. B. Siekmann, H. Bunjes, M. H. J. Koch, and K. Westesen. Preparation and structural investigations of colloidal dispersions prepared from cubic monoglyceride–water phases. *Int. J. Pharm.* **244**:33–43 (2002).
13. J. S. Kim, H. K. Kim, H. Chung, Y. T. Sohn, I. C. Kwon, and S. Y. Jeong. Drug formulations that form a dispersed cubic phase when mixed with water. *Proc. Int. Symp. Control. Release Bioact. Mater.* **27**:1118–1119 (2000).
14. P. T. Spicer and K. L. Hayden. Novel process for producing cubic liquid crystalline nanoparticles (cubosomes). *Langmuir* **17**:5748–5756 (2001).
15. J. Gustafsson, H. Ljusberg-Wharen, M. Almgrem, and K. Larsson. Cubic lipid–water phase dispersed into submicron particles. *Langmuir* **12**:4611–4613 (1996).
16. E. Esposito, N. Eblovi, S. Rasi, M. Drechsler, G. M. Di Gregorio, E. Menegatti, R. Cortesi. Lipid-based supramolecular systems for topical application: a preformulatory study. *AAPS PharmSci.* 5(4) article 30 (2003).
17. N. Lars and A.-A. Ashraf. Stratum corneum keratin structure, function, and formation: the cubic rod-packing and membrane templating model. *J. Invest. Dermatol.* **4**:715–732 (2004).
18. M. Nakano, A. Sugita, H. Matsuoka, and T. Handa. Small angle X-ray scattering and ^{13}C NMR investigation on the internal structure of "cubosomes." *Langmuir* **17**:3917–3922 (2001).
19. M. Almgrem, K. Edwards, and G. Karlsson. Cryo transmission electron microscopy of liposomes and related structures. *Colloids Surf., A* **174**:3–21 (2000).
20. S. Engstrom, B. Ericsson, and T. Landh. A cubosome formulation for intravenous administration of somatostatin. *Proc. Int. Symp. Control. Release Bioact. Mater.* **23**:382–383 (1996).
21. J. S. Kim, H. K. Kim, H. Chung, Y. T. Sohn, I. C. Kwon, and S. Y. Jeong. Drug formulations that form a dispersed cubic phase when mixed with water. *Proc. Int. Symp. Control. Release Bioact. Mater.* **27**:1118–1119 (2000).
22. J. B. Boyd. Characterisation of drug release from cubosomes using the pressure ultrafiltration method. *Int. J. Pharm.* **260**: 239–247 (2000).
23. K. C. Kwan, G. O. Breault, E. R. Umbenhauer, F. G. McMahon, and D. E. Duggan. Kinetics of indomethacin absorption, elimination, and enterohepatic circulation in man. *J. Pharm. Biopharm.* **4**:255–280 (1976).
24. L. Helleberg. Clinical pharmacokinetics of indomethacin. *Clin. Pharmacokinet.* **6**:245–258 (1981).
25. P. Srinath, M. G. Chary, S. P. Vyas, and P. V. Diwan. Long circulating liposomes of indomethacin in arthritic rats—a biodisposition study. *Pharm. Acta Helv.* **74**:399–404 (2000).
26. C. Puglia, D. Trombetta, V. Venuti, A. Saija, and F. Bonina. Evaluation of *in vitro* topical anti-inflammatory activity of indomethacin from liposomal vesicles. *J. Pharm. Pharmacol.* **56**:1225–1232 (2004).
27. S. Miyazaki, A. Takahashi, W. Kubo, J. Bachynsky, and R. Lobenberg. Poly *n*-butylcyanoacrylate (PNBCA) nanocapsules as a carrier for NSAIDs: *in vitro* release and *in vivo* skin penetration. *J. Pharm. Pharm. Sci.* **6**:238–245 (2003).
28. M. H. Moon, I. Park, and Y. Kim. Size characterization of liposomes by flow field-flow fractionation and photon correlation spectroscopy. Effect of ionic strength and pH of carrier solutions. *J. Chromatogr., A* **813**:91–100 (1998).
29. C. Contado and F. Dondi. Barley starch granules subject to SPLITT cell fractionation and Sd/StFFF size characterization. *Starch* **53**:414–423 (2001).
30. S. Liu, M. Kamijo, T. Takayasu, and S. Takayama. Direct

analysis of indomethacin in rat plasma using a column-switching high-performance liquid chromatographic system. *J. Chromatogr., B* **767**:53–60 (2002).
31. R. L. Bronaugh, R. F. Stewart, and M. Simon. Methods for *in vitro* percutaneous absorption studies VII: use of excised human skin. *J. Pharm. Sci.* **75**:1094–1097 (1986).
32. M. Bouclier, A. Chatelus and C. N. Hensby. *In vivo* animal models for the evaluation of anti-inflammatory drug action in the skin. In N.J. Lowe and C.N. Hensby (eds.), *Nonsteroidal Anti-inflammatory Drugs*, Karger, Basel, 1989, pp. 118–132.
33. E. Touitou and B. Fabin. Altered skin permeation of a highly lipophilic molecule: tetrahydrocannabinol. *Int. J. Pharm.* **43**:17–22 (1988).
34. M. Ricci, C. Puglia, F. Bonina, C. Di Giovanni, S. Giovagnoli, and C. Rossi. Evaluation of indomethacin percutaneous absorption from nanostructured lipid carriers (NLC): *in vitro* and *in vivo* studies. *J. Pharm. Sci.* **94**:1149–1159 (2005).
35. A. Saija, A. Tomaino, D. Trombetta, A. De Pasquale, N. Uccella, T. Barbuzzi, D. Paolino, and F. Bonina. *In vitro* and *in vivo* evaluation of caffeic and ferulic acids as topical photoprotective agents. *Int. J. Pharm.* **199**:39–47 (2000).
36. J. B. Dawson, D. J. Barker, D. J. Ellis, E. Grassam, J. A. Catterill, G. W. Fischer, and J. W. Feather. A theoretical and experimental study of light absorption and scattering by *in vivo* skin. *Phys. Med. Biol.* **25**:696–709 (1980).
37. G. Wörle, K. Westesen, M. H. J. Koch. Investigation of the phase behavior of monoolein/surfactant dispersions of different composition and preparation methods. *EMBL Hamburg Outstation Annual Report* (2000).
38. M. Schimpf, K. Caldwell and J. C. Giddings. *Field-Flow Fractionation Handbook*, Wiley-Interscience, New York, 2000.
39. S. Levin and E. Klausner. Measurements of size distribution and density of pharmaceutical fat emulsions, using field-programmed sedimentation field-flow fractionation (SdFFF). *Pharm. Res.* **12**: 1218–1224 (1995).
40. S. Levin, R. Nudelman, P. Reschiglian, and L. Pasti. Simulation of fractograms of fat emulsions in power-programmed sedimentation field-flow fractionation (SdFFF). *J. Pharm. Biomed. Anal.* **13**:869–877 (1995).
41. G. Lu and H. W. Jun. Diffusion studies of methotrexate in carbopol and poloxamer gels. *Int. J. Pharm.* **160**:1–9 (1998).
42. J. J. van de Sandt, J. A. van Burgsteden, S. Cage, P. L. Carmichael, I. Dick, S. Kenyon, G. Korinth, F. Larese, J. C. Limasset, W. J. Maas, L. Montomoli, J. B. Nielsen, J. P. Payan, E. Robinson, P. Sartorelli, K. H. Schaller, S. C. Wilkinson, and F. M. Williams. *In vitro* predictions of skin absorption of caffeine, testosterone, and benzoic acid: a multi-centre comparison study. *Regul. Toxicol. Pharmacol.* **39**:271–281 (2004).
43. F. P. Bonina, C. Puglia, T. Barbuzzi, P. de Caprariis, F. Palagiano, M. G. Rimoli, and A. Saija. *In vitro* and *in vivo* evaluation of polyoxyethylene esters as dermal prodrugs of ketoprofen, naproxen and diclofenac. *Eur. J. Pharm. Sci.* **14**:123–134 (2001).